The structure of molten AgCl, AgI and their eutectic mixture as studied by molecular dynamics simulations of polarizable ion model potentials

ARTICLE *in* THE JOURNAL OF CHEMICAL PHYSICS · JANUARY 2011

Impact Factor: 2.95 · DOI: 10.1063/1.3506867 · Source: PubMed

3 AUTHORS:

Olga Alcaraz
Polytechnic University of Catalonia
19 PUBLICATIONS **149** CITATIONS
SEE PROFILE

Vicente Bitrián
Polytechnic University of Catalonia
12 PUBLICATIONS **112** CITATIONS
SEE PROFILE

Joaquim Trullàs Simó
Polytechnic University of Catalonia
37 PUBLICATIONS **451** CITATIONS
SEE PROFILE

The structure of molten AgCl, AgI and their eutectic mixture as studied by molecular dynamics simulations of polarizable ion model potentials

Olga Alcaraz, Vicente Bitrián, and Joaquim Trullàs[a)]
Departament de Física i Enginyeria Nuclear, Universitat Politècnica de Catalunya, Campus Nord UPC B4-B5, 08034 Barcelona, Spain

(Received 5 August 2010; accepted 7 October 2010; published online 5 January 2011)

The structure of molten AgCl, AgI, and their eutectic mixture $Ag(Cl_{0.43}I_{0.57})$ is studied by means of molecular dynamics simulations of polarizable ion model potentials. The corresponding static coherent structure factors reproduce quite well the available neutron scattering data. The qualitative behavior of the simulated partial structure factors and radial distribution functions for molten AgCl and AgI is that predicted by the reverse Monte Carlo modeling of the experimental data. The AgI results are also in qualitative agreement with those calculated from *ab initio* molecular dynamics. © *2011 American Institute of Physics*. [doi:10.1063/1.3506867]

I. INTRODUCTION

Silver and copper halides MX (M = Ag, Cu; X = I, Br, Cl) exhibit fast-ion conductivity in their solid phase, namely, their ionic conductivities at high temperatures ($\sim 1\ \Omega^{-1}\ cm^{-1}$) are of the same order as in the liquid phase.[1–3] At ambient temperature, AgI, CuI, and CuBr form the γ phase with zinc-blende structure. They also form the β phase with wurtzite structure. However, while the γ and β phases of AgI are stable at the same temperature, CuI and CuBr undergo a transformation from the γ to the β phase at 642 and 664 K, respectively. Furthermore, at higher temperatures (420 K for AgI, 680 K for CuI, and 744 K for CuBr) the three salts experience a first order transition to the superionic α phase, where the anions of AgI and CuBr form a bcc lattice and those of CuI an fcc lattice with Ag^+ or Cu^+ the mobile species. From this phase AgI melts at 829 K, CuI at 878 K, and CuBr at 765 K. On the other hand, although AgBr, AgCl, and CuCl also exhibit a relatively high ionic conductivity before melting, they are not regarded as true superionic conductors. CuCl also forms the γ phase with zinc-blende structure at ambient temperature and transforms to the wurtzite β phase at 681 K. As the temperature increases, the Frenkel defects concentration increases in such a way that some cations jump up from their tetrahedral sites to the free tetrahedral interstitial sites and the ionic conductivity increases up to $\approx 0.1\ \Omega^{-1}\ cm^{-1}$ before melting at 703 K without any first order phase transition in between. AgBr and AgCl are stable in the ambient rock-salt structure up to their melting points at 701 and 728 K, respectively. However, from 100 to 150 K below the melting, they also exhibit rapid increases in their ionic conductivities due to the Frenkel defects formation. AgBr, AgCl, and CuCl are not regarded as true superionic conductors because the Frenkel defects concentration is much lower than in superionic fluorites.[3]

The superionic behavior of α-AgI and α-CuI was reproduced by Vashishta and Rahman[4,5] by molecular dynamics (MD) simulations using simple effective pair potentials. The two main characteristics of these rigid ion potentials, which we will denote as VR, are: (i) the absolute value of effective charges is lower than e and (ii) the anionic radius is about the double than the cationic one. By using a refined parameterization of the original VR potential, Parrinello, Rahman, and Vashishta[6] (PRV) carried out MD simulations of the β–α transition in AgI. This particular VR potential, with the refined parameter values, has been widely used to study solid AgI.[7–9]

Howe *et al.*,[10] following their diffuse neutron scattering data, noted the similarity between the α-AgI structure and that of molten CuCl[11,12] and conjectured that superionic systems have similar structure in the molten phase. This idea prompted Stafford and Silbert[13] to carry out theoretical calculations of the radial distribution functions and structure factors of molten AgI within the hypernetted chain (HNC) approximation by using the PRV potential. Their results turned out to qualitatively agree with the experimental static structure factor $S(k)$ available shortly after,[14] despite some differences in the quantitative sense. Furthermore, Stafford *et al.*[15] parameterized VR potentials for CuBr and CuCl and carried out HNC and MD calculations. Their results for the structure factors of molten CuCl reproduce quite well the main features of the measured functions.[11,12,16] Silbert and co-workers also parameterized VR potentials for AgBr and AgCl,[17] but the calculated $S(k)$ failed to reproduce the three-peak fine structure present in the broad main peak of the available experimental data.[18–20] At the same time, Wilson *et al.*[21] showed by MD simulations that this structure can be predicted for molten AgCl, although it is overestimated, if polarizable ion model (PIM) potentials are considered. They studied model potentials where the many-body interactions due to the induced dipole and quadrupole polarization are added to the rigid ion pair potential of the Born–Mayer form proposed by Mayer[22] for AgCl. They introduced the induced quadrupole contributions because they also studied the hot solid phase of AgCl, where there are large cancellations of the dipole contributions on account of crystal symmetry. Later, Trullàs *et al.*[23–25] showed that the three-peak structure of molten AgCl and AgBr can also be reproduced if the anion induced dipole polarization contributions are added to VR potentials.

a)Author to whom correspondence should be addressed. Electronic mail: quim.trullas@upc.edu.

Moreover, Bitrian *et al.*[26–29] have shown that the inclusion of the anions polarizability in VR potentials accounts for the experimental prepeak at about 1 $Å^{-1}$ of the $S(k)$ for molten AgI.

Since more recent experimental structure factors for molten AgCl and AgI and their eutectic mixture $Ag(Cl_{0.43}I_{0.57})$ are now available,[30] together with the radial distribution functions predicted by the reverse Monte Carlo (RMC) modeling of the corresponding neutron scattering data,[31,32] as well as *ab initio* MD results of molten AgI,[33] the purpose of the present paper is to study the structure of these systems by MD of PIM. Beyond the structural properties of the mixture between molten AgCl and AgI, their dynamic properties were studied by sound absorption.[34]

The layout of this paper is as follows. We describe the PIM in Sec. II and give some details of MD simulations in Sec. III. We present and discuss the results in Sec. IV and summarize them in the concluding remarks of Sec. V.

II. POLARIZABLE IONS MODELS

We use the PIM defined in our previous works,[24,25,27] which can be briefly described as follows. The system is made up of ions, each one with a point charge q_i and an inducible point dipole whose moment is given by

$$\boldsymbol{\mu}_i = \alpha_i \mathbf{E}_i = \alpha_i \left(\mathbf{E}_i^{\mathrm{q}} + \mathbf{E}_i^{\boldsymbol{\mu}}\right), \tag{1}$$

where α_i is the electronic polarizability and $\mathbf{E}_i = \mathbf{E}_i^{\mathrm{q}} + \mathbf{E}_i^{\boldsymbol{\mu}}$ is the local electric field at the ionic position $\mathbf{r}_i$, with $\mathbf{E}_i^{\mathrm{q}}$ the field created by all point charges except q_i and $\mathbf{E}_i^{\boldsymbol{\mu}}$ the field due to all dipole moments except $\boldsymbol{\mu}_i$. The ions interact through effective pair potentials of the form

$$\phi_{ij}^0(r_{ij}) = \frac{z_i z_j e^2}{r_{ij}} + \frac{H_{ij}}{r_{ij}^{\eta_{ij}}} - \frac{C_{ij}}{r_{ij}^6} \tag{2}$$

with

$$H_{ij} = A(\sigma_i + \sigma_j)^{\eta_{ij}} \quad \text{and} \quad C_{ij} = \frac{3}{2}\alpha_i \alpha_j \frac{W_i W_j}{W_i + W_j}. \tag{3}$$

The first term in Eq. (2) is the Coulomb interaction between charges with z_i the effective charge in units of the fundamental charge e ($q_i = z_i e$). The second term models the repulsion between the ions with H_{ij} given in Eq. (3), where σ_i are related to the ionic radii, A defines the strength and η_{ij} the hardness of the repulsive interactions. The third term is the van der Waals contribution with C_{ij} in Eq. (3), where W_i are related to the appropriate average excitation energies. Since we assume $\alpha_{\mathrm{Ag}} = 0$, we have $C_{\mathrm{AgAg}} = C_{\mathrm{AgCl}} = C_{\mathrm{AgI}} = 0$. Hence, the potential energy of the PIM is that due to the rigid ion potential interactions plus that due to the many-body induced polarization interactions, which can be written as

$$U = \frac{1}{2}\sum_{i=1}^{N}\sum_{j\neq i}^{N}\phi_{ij}^0(r_{ij}) - \sum_{i=1}^{N}\boldsymbol{\mu}_i \cdot \mathbf{E}_i^{\mathrm{q}} - \frac{1}{2}\sum_{i=1}^{N}\boldsymbol{\mu}_i \cdot \mathbf{E}_i^{\boldsymbol{\mu}} + \sum_{i=1}^{N}\frac{\mu_i^2}{2\alpha_i}. \tag{4}$$

We note that the PIM used in this work do not include the short-range damping polarization studied in Refs. 25 and 27.

TABLE I. Potential parameters.

	AgCl	AgI	$Ag(Cl_{0.43}I_{0.57})$
z_{Ag}	0.68	0.58	0.62
z_{Cl}	−0.68	...	−0.62
z_{I}	...	−0.58	−0.62
η_{AgAg}	6	11	8.85
η_{AgCl}	6	...	6.00
η_{ClCl}	6	...	6.00
η_{AgI}	...	9	9.00
η_{ClI}	...	...	6.57
η_{II}	...	7	7.00
A (eV)	0.1418	0.1418	0.1418
σ_{Ag} (Å)	0.856	0.506	0.656
σ_{Cl} (Å)	2.06		2.06
σ_{I} (Å)	...	2.252	2.252
W_{Cl} (eV)	9.75	...	9.75
W_{I} (eV)	...	3.00	3.00
α_{Ag} ($Å^3$)	0	0	0
α_{Cl} ($Å^3$)	3.45	...	3.45
α_{I} ($Å^3$)	...	6.12	6.12

The values of the potential parameters used in this work for AgCl, AgI, and their eutectic mixture $Ag(Cl_{0.43}I_{0.57})$ are given in Table I. The values for AgI are obtained from those proposed by Shimojo and Kobayashi,[35] who slightly modified the parameterization of Parrinello, Rahman, and Vashishta[6] in order to reproduce the α-phase features at the appropriate experimental density. In fact, Ref. 35 gives the values of the three H_{ij} in place of the values of A and the two radii σ_i, but the latter can be derived from the former by solving the corresponding three-equation system. The values for AgCl are obtained from Ref. 17, where the three values of H_{ij} are given together with those of the two radii, in such a way that the A value is easily derived. However, because the three hardness parameters η_{ij} for AgCl has the same value, the values of A, σ_{Ag}, and σ_{Cl} can be rescaled to get the same values of H_{ij}. Then, in order to simplify the parametrization of the potentials in the liquid mixture (see below), we rescaled σ_{Ag} and σ_{Cl} to get for AgCl the same value of A as for AgI.

The potential parameters for pure AgI and AgCl do not determine the interaction potentials for their mixtures because for each pure salt we have different values for the effective charges z_i, the cationic radius σ_{Ag}, and the hardness parameters η_{ij}. Then, we assume that these values for the mixture are a linear combination of the pure values weighted by the concentration, namely, the value p of z_i, σ_{Ag}, or η_{ij} in the mixture is $p = x_{\mathrm{AgCl}}\, p_{\mathrm{AgCl}} + x_{\mathrm{AgI}}\, p_{\mathrm{AgI}}$, where x_{AgCl} and $x_{\mathrm{AgI}} = 1 - x_{\mathrm{AgCl}}$ are the concentration of AgCl and AgI, respectively, and p_{AgCl} and p_{AgI} are the values of the parameters for the corresponding pure salt. The use of the linear combination of the potentials of the pure melts is inspired by the previous work on molten $Ag(Br_{0.7}I_{0.3})$,[36] where it was found that the total structure factor of the mixture can be constructed from the linear combination of those for the pure cases. The parameter values obtained with $x_{\mathrm{AgCl}} = 0.43$ and $x_{\mathrm{AgI}} = 0.57$ are those in Table I. Note that the anionic polarizability values in the mixture, $\alpha_{\mathrm{Cl}} = 3.45$ $Å^3$ and $\alpha_{\mathrm{I}} = 6.12$ $Å^3$ (with $\alpha_{\mathrm{Ag}} = 0$), are the same as for the pure melts.

III. MD SIMULATIONS DETAILS

By using the PIM described above, we have simulated molten AgCl at 773 K, molten AgI at 923 K, and the molten mixture $Ag(Cl_{0.43}I_{0.57})$ at 743 K, the temperatures at which more recent neutron diffraction data are available.[30] The ionic number densities $\rho = N/V$ (N is the number of ions in a volume V) given in Ref. 37 for molten AgCl and AgI are 0.0406 and 0.0281 ions/Å^3, respectively. For $Ag(Cl_{0.43}I_{0.57})$ we assume $\rho = 0.03405$ Å^{-3}. This value has been estimated by the linear relation $\rho(T) = 0.43\rho_{AgCl}(T) + 0.57\rho_{AgI}(T)$, where $\rho_{AgCl}(T)$ and $\rho_{AgI}(T)$ are the ionic densities at temperature $T = 743$ K given in Ref. 37 for AgCl and AgI, respectively.

We have also carried out complementary MD simulations of a rigid ion model (RIM) potential for molten AgCl where the ions interact solely through effective pair potentials of the VR form $\phi_{ij}(r_{ij}) = \phi^0_{ij}(r_{ij}) - P_{ij}/r^4_{ij}$, where $P_{ij} = (\alpha_i z_j^2 + \alpha_j z_i^2)e^2/2$ (Ref. 4) with the values of z_i and α_i given above. The term $-P_{ij}/r^4_{ij}$ models in some sense the effective monopole-induced dipole interactions due to the anion polarizability. Hereafter, the results from MD simulations using PIM or RIM will be denoted as polarizable ion model-molecular dynamics (PIM-MD) or rigid ion model-molecular dynamics (RIM-MD), respectively.

MD simulations have been carried out with 500 cations and 500 anions (215 bromides and 285 iodides in the case of the eutectic mixture), placed in a cubic box of side $L = (N/\rho)^{1/3}$ with periodic boundary conditions. Computational details are those described in previous papers.[24,25,27]

The basic structural properties calculated in the simulations are the radial distribution functions $g_{ab}(r)$ and the Ashcroft–Langreth partial structure factors $S_{ab}(k)$, which are related by the Fourier transform

$$S_{ab}(k) = \delta_{ab} + \rho\sqrt{c_a c_b}\int_0^\infty [g_{ab}(r) - 1]\frac{\sin(kr)}{kr}4\pi r^2 dr, \tag{5}$$

where δ_{ab} is the Kronecker's delta and $c_a = N_a/N$ is the ionic number concentration of species a with N_a the number of ions of species a and $N = \Sigma_a N_a$. Since $g_{ab}(r)$ still oscillate at the largest distances accessible by MD simulations, the corresponding $S_{ab}(k)$ at low k's cannot be calculated using Eq. (5) because this method gives spurious oscillations due to truncation errors. Then, the calculations for $k < 4$ Å^{-1} have been carried out directly using

$$S_{ab}(k) = \frac{1}{N\sqrt{c_a c_b}}\left\langle \sum_{ia=1}^{Na} \exp(i\mathbf{k}\cdot\mathbf{r}_{ia}) \sum_{jb=1}^{Nb} \exp(-i\mathbf{k}\cdot\mathbf{r}_{jb})\right\rangle, \tag{6}$$

where the angular brackets denote the ensemble average over the equilibrium configurations, $\mathbf{r}_{ia}$ is the position of the particle ia of species a, and $\mathbf{k} = (2\pi/L)\mathbf{n}$ is a wave vector in the reciprocal space allowed by the periodic boundary conditions with $\mathbf{n}$ a vector with integer components. While good $g_{ab}(r)$ are obtained averaging over 10^4 configurations, long simulations of 10^6 time steps are required to get $S_{ab}(k)$ with small uncertainties for $k < 4$ Å^{-1}. The structure factor of the intensity of neutron radiation coherently scattered is constructed from the partials as[38]

$$S(k) = \frac{1}{b^2}\sum_a\sum_b b_a b_b\sqrt{c_a c_b}S_{ab}(k), \tag{7}$$

where b_a are the coherent neutron scattering lengths and $b^2 = \Sigma_a c_a b_a^2$. The values of b_a used in our work are, in femtometers (10^{-15} m), those of Ref. 39: $b^{nat}_{Ag} = 5.922$, $b^{nat}_{Cl} = 9.577$, and $b^{nat}_{I} = 5.280$. The structure factor in Eq. (7) is normalized in such a way that it goes to 1 as $k \to \infty$. It should not be confused with $F(k) = b^2[S(k) - 1]$, which is usually defined in terms of the Faber–Zimman partial structure factors $A_{ab}(k) = (c_a c_b)^{-1/2}[S_{ab}(k) - \delta_{ab}] + 1$.[16,40,41] Note that the partials published in Refs. 31 and 32 are the Faber–Zimman structure factors.

IV. RESULTS

A. Structure of molten AgCl

In Fig. 1 we compare the $S(k)$ for molten AgCl from PIM-MD and RIM-MD with those obtained from neutron scattering (NS) measurements by Kawakita *et al.*[30] and by Tahara *et al.*[31] The two experiments were carried out using a pulse neutron and HIT-II time of flight spectrometer. However, Tahara *et al.* complemented their data at low k's with those obtained by using a monochromatic neutron beam in the HERMES high resolution diffractometer. This could be the reason why the NS results are different for $k < 1.5$ Å^{-1}. While the $S(k)$ by Kawakita *et al.* fluctuates at around 0.18 at low k's that by Tahara *et al.* decreases to 0 as $k \to 0$. For $k > 1.5$ Å^{-1}, both experimental sets of data are almost identical within the small fluctuating uncertainties. They present a broad and flattened main peak with a small spiky peak at about 1.9 Å^{-1}, a maximum at about 3.2 Å^{-1}, and a hump in between. Tahara *et al.* locate the hump at about 2.8 Å^{-1}, while Kawakita *et al.* locate it at about 2.5 Å^{-1}. This three-peak fine structure is clearer in the earlier experimental $S(k)$ obtained by Derrien and Dupuy.[18] Concerning the $S(k)$ from

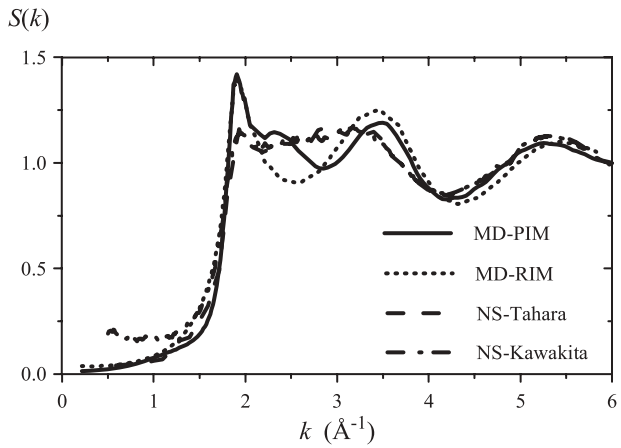

FIG. 1. The structure factor $S(k)$ for molten AgCl from PIM-MD (solid line) and RIM-MD (dotted line) of this work and from NS measurements by Tahara *et al.* (Ref. 31) (dashed line) and by Kawakita *et al.* (Ref. 30) (dash-dot line).

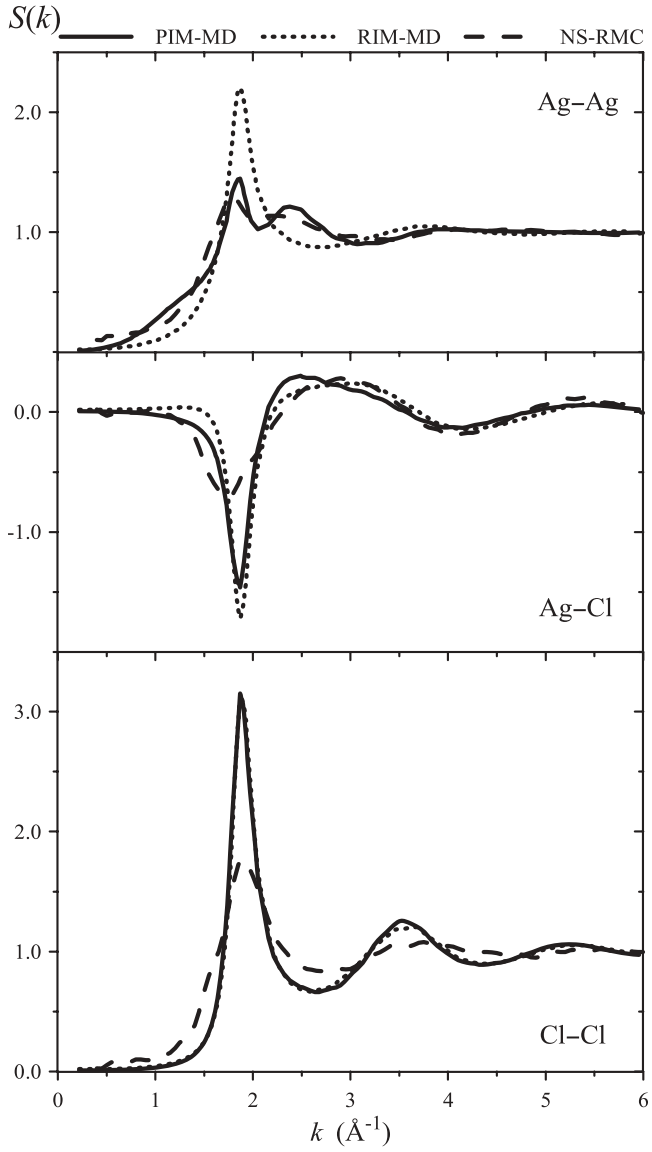

FIG. 2. The Ashcroft–Langreth partial structure factors $S_{AgAg}(k)$ (top), $S_{AgCl}(k)$ (middle), and $S_{ClCl}(k)$ (bottom) for molten AgCl from PIM-MD (solid line) and RIM-MD (dotted line) of this work and from NS-RMC by Tahara *et al.* (Ref. 31) (dashed line).

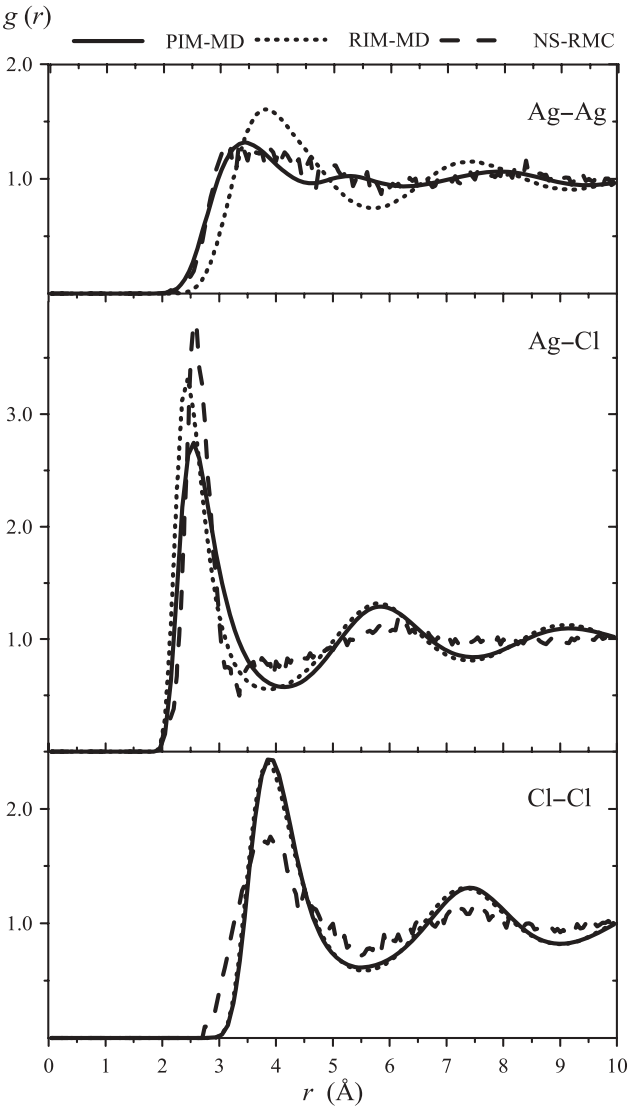

FIG. 3. The radial distribution functions $g_{AgAg}(r)$ (top), $g_{AgCl}(r)$ (middle), and $g_{ClCl}(r)$ (bottom) for molten AgCl from PIM-MD (solid line) and RIM-MD (dotted line) of this work and from NS-RMC by Tahara *et al.* (Ref. 31) (dashed line).

PIM-MD, although the three-peak structure is overestimated, the agreement with experimental results is fairly good, at least better than for RIM-MD. At low k's the simulated $S(k)$ are very close to that by Tahara *et al.*

In Fig. 2 we show the PIM-MD and RIM-MD results for the Ashcroft–Langreth partial structure factors $S_{ab}(k)$ of molten AgCl and those obtained by Tahara *et al.*[31] using the RMC analysis of their NS data (NS-RMC). In the three cases, $S_{ClCl}(k)$ presents the first large peak and $S_{AgCl}(k)$ the deep first valley, at about 1.9 Å^{-1}, which are less pronounced for NS-RMC because the oscillations of the corresponding $g_{ClCl}(r)$ and $g_{AgCl}(r)$ are less pronounced (see Fig. 3 below). Regarding $S_{AgAg}(k)$, those from PIM-MD and NS-RMC are less structured with a peak at about 1.9 Å^{-1} and a hump at about 2.4 Å^{-1}, which are slightly more pronounced for PIM-MD. The hump leads to the middle feature of the three-peak fine structure in $S(k)$. The $S_{AgAg}(k)$ from RIM-MD only presents a peak at about 1.9 Å^{-1}, in such a way that the corresponding $S(k)$ has a valley between two peaks at about 1.9 and 3.4 Å^{-1}. The origin of the middle hump can be understood by looking at the radial distribution functions plotted in Fig. 3.

The $g_{ClCl}(r)$ and $g_{AgCl}(r)$ from PIM-MD, RIM-MD, and NS-RMC oscillate in opposite phase, showing that a chloride is surrounded by alternated shells of opposite charged ions as in molten alkali halides. These oscillations, whose wavelength is about 3.4 Å, lead to the large first peak and the deep first valley in $S_{ClCl}(k)$ and $S_{AgCl}(k)$, respectively, at about $2\pi/(3.4\ \text{Å}) \approx 1.9$ Å^{-1}. However, the $g_{AgAg}(r)$ from PIM-MD and NS-RMC are not in phase with $g_{ClCl}(r)$ as in RIM-MD. Both $g_{AgAg}(r)$ from PIM-MD and NS-RMC are structureless with the first peak at about 3.4 Å between the first peak positions of $g_{AgCl}(r)$ and $g_{ClCl}(r)$. Moreover, in the PIM-MD $g_{AgAg}(r)$, it can be appreciated that (a) its second peak is at about 5.3 Å, between the first and second peaks of $g_{AgCl}(r)$, i.e., around each cation there is a double shell of cations

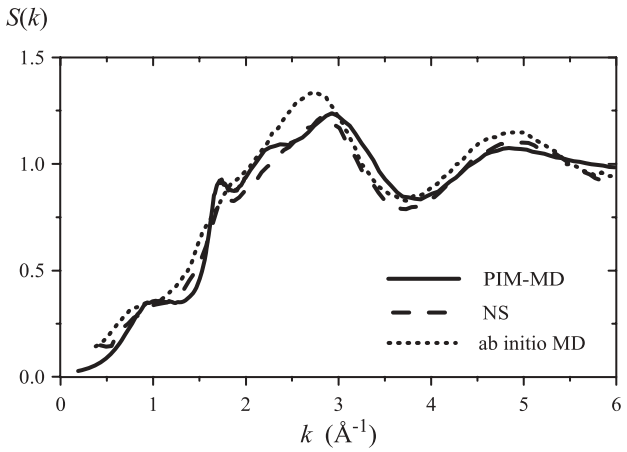

FIG. 4. The structure factor $S(k)$ for molten AgI from PIM-MD of this work (solid line), NS measurements by Kawakita *et al.* (Ref. 30) (dashed line), and *ab initio* MD by Shimojo *et al.* (Ref. 33) (dotted line).

between the first and second shells of anions and (b) its third peak position is at about 8.0 Å, at a larger value of r than the second peak position of $g_{\mathrm{ClCl}}(r)$. The *wavelength* of 2.7 Å between the second and third peaks of $g_{\mathrm{AgAg}}(r)$ leads to the hump of $S_{\mathrm{AgAg}}(k)$ at about $2\pi/(2.7\ \text{Å}) \approx 2.4\ \text{Å}^{-1}$, which in turn leads to the middle hump in $S(k)$. Although less clear, it appears that within the fluctuating uncertainties, the $g_{\mathrm{AgAg}}(r)$ from NS-RMC also follows this behavior. Beyond the third peak, the distances between two consecutives relative maxima in the $g_{\mathrm{AgAg}}(r)$ from PIM-MD is about 3.4 Å, the *wavelength* that leads to the first peak in $S_{\mathrm{AgAg}}(k)$ at about 1.9 Å^{-1}.

The PIM-MD $g_{\mathrm{AgAg}}(r)$ first peak position at shorter distances than that from RIM-MD can be attributed to the screening of the repulsion between cations due to the induced polarization in the anions, in such a way that the separation between two cations can be smaller than it would be if the anions were not polarized, and the first shell of cations around a cation in RIM-MD splits into a double shell of cations in PIM-MD.

B. Structure of molten AgI

In Fig. 4 we compare the $S(k)$ calculated for molten AgI from PIM-MD with that obtained by Kawakita *et al.*[30] from NS measurements, which are those also published in Ref. 36. The agreement between them is really good. Both PIM-MD and NS results present a prepeak at about 1 Å^{-1} and a broad main peak between a small spiky feature at about 1.7 Å^{-1} and the highest value at about 2.9 Å^{-1}. However, the $S(k)$ from PIM-MD shows a mid shoulder at about 2.3 Å^{-1} which is not appreciable in the NS results and the highest value from PIM-MD is slightly displaced toward a higher k with respect to the scattering data.

Earlier experimental $S(k)$ for molten AgI,[14,20,42] which were obtained by using a monochromatic neutron beam and a two axis diffractometer in place of a pulse neutron and a time of flight spectrometer as Kawakita *et al.*, also exhibit the prepeak and the broad main peak. However they present some differences. The earlier experimental $S(k)$ obtained by Inui *et al.*[20] show a main peak higher than in Fig. 4. It is because they used multiple scattering corrections in the thermodynamic limit, while later data have been corrected with the Blech and Averbach method. The height of the main peak in the $S(k)$ published by Shirakawa *et al.*,[42] which follows from the original NS data of Inui *et al.*[20] but corrected with the Blech and Averbach method, is similar to that in Fig. 4. However, the values of this $S(k)$ before the spiky like feature are lower than those in Fig. 4. It could be because the Kawakita *et al.*[30] results in Fig. 4 were not asymptotically extrapolated to the thermodynamic value of $S(0)$ by renormalizing the observed $S(k)$.[36]

Shimojo *et al.*[33] carried out *ab initio* MD of molten AgI at 950 K and calculated $S(k)$ from the partials. Their $S(k)$ is in excellent agreement with the NS data published by Kawakita *et al.* in Ref. 32, so excellent that differences between them are hard to see at first sight. As can be seen in Fig. 4, the *ab initio* $S(k)$, and then that by Kawakita *et al.* in Ref. 32, although slightly higher, are very close to the NS data by Kawakita *et al.* in Ref. 30. In Fig. 5 we compare the *ab initio* and PIM-MD results for $S_{ab}(k)$ as well as those obtained by Kawakita *et al.* in Ref. 32 from NS-RMC.

In spite of the excellent agreement between the *ab initio* and experimental $S(k)$ in Ref. 32, there are some differences between the corresponding $S_{ab}(k)$. For instance, the first peak at about 1.7 Å^{-1} of the *ab initio* $S_{\mathrm{II}}(k)$ is lower than that obtained from NS-RMC. Moreover, at this peak position, the *ab initio* $S_{\mathrm{AgAg}}(k)$ presents a relative maximum while that from NS-RMC shows a relative minimum. These differences illustrate the fact that two different sets of partials can lead to the same $S(k)$. Concerning the PIM-MD results, the first peak of $S_{\mathrm{II}}(k)$ is higher, and the main valley of $S_{\mathrm{AgI}}(k)$ is deeper, than in *ab initio* or NS-RMC results. Nevertheless, the qualitative behavior of the partials is the same for the three sets of data. The shape of $S_{\mathrm{II}}(k)$ and $S_{\mathrm{AgI}}(k)$, with a large first peak and a deep first valley, respectively, at about 1.7 Å^{-1}, is that expected for charge-ordered liquids such as molten alkali halides and that seen above for molten AgCl. On the other hand, $S_{\mathrm{AgAg}}(k)$ is flatter and has a prepeak at about 1 Å^{-1}. This prepeak, which is not seen in molten AgCl, reflects the spatial correlations between cations on an intermediate length scale around $2\pi/(1\ \text{Å}^{-1})$ resulting from the inhomogeneous cationic distribution.[26] The $S_{\mathrm{AgAg}}(k)$ from PIM-MD is very close to that from *ab anitio* MD, with two relative maxima at about 1.7 and 2.3 Å^{-1}, which are more pronounced in the former. This special profile of $S_{\mathrm{AgAg}}(k)$ leads to the $S(k)$ with the prepeak and the broad main peak. The mid shoulder in the broad main peak of the $S(k)$ from PIM-MD is a signature of the $S_{\mathrm{AgAg}}(k)$ maximum at 2.3 Å^{-1}, which is not detectable in the *ab initio* $S(k)$.

In Fig. 6 we compare the $g_{ab}(r)$ from PIM-MD, *ab initio* MD, and NS-RMC. In spite of the differences, the qualitative behavior of these functions is almost the same for the three sets of data, and it is similar to that found for molten AgCl but with I in place of Cl. In all the cases $g_{\mathrm{II}}(r)$ and $g_{\mathrm{AgI}}(r)$ oscillate in opposite phase with a *wavelength* of about 3.7 Å and wave number $2\pi/(3.7\ \text{Å}) \approx 1.7\ \text{Å}^{-1}$, while the smaller oscillations of $g_{\mathrm{AgAg}}(r)$ are not in phase with those in $g_{\mathrm{II}}(r)$. The first peak

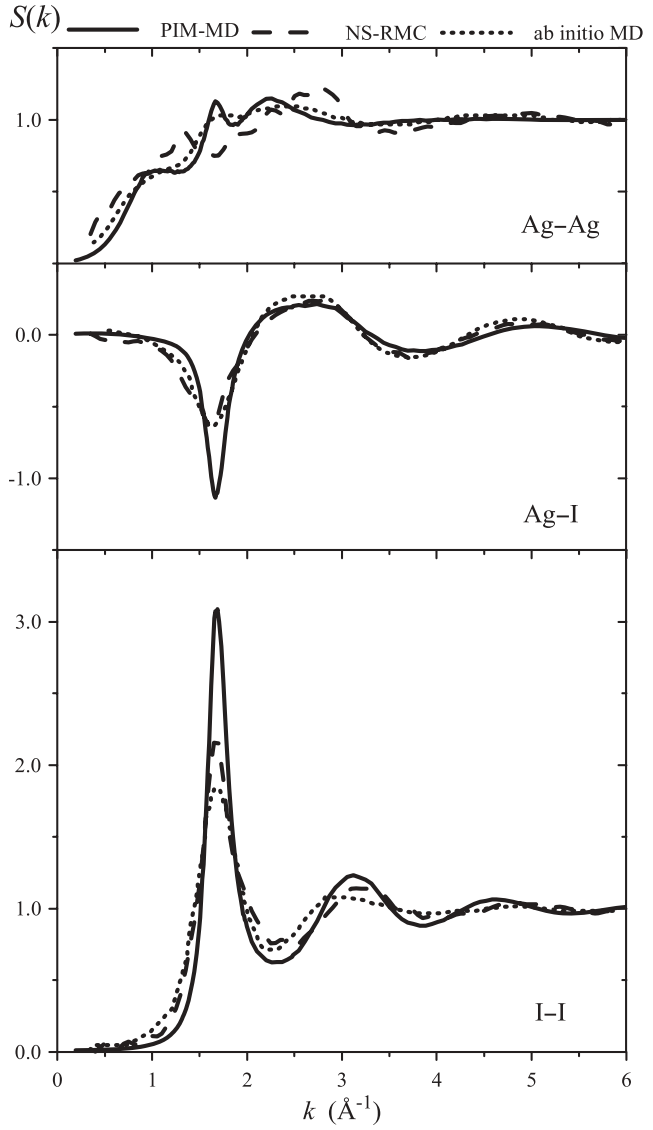

FIG. 5. The Ashcroft–Langreth partial structure factors $S_{AgAg}(k)$ (top), $S_{AgI}(k)$ (middle), and $S_{II}(k)$ (bottom) for molten AgI from PIM-MD of this work (solid line), NS-RMC by Kawakita *et al.* (Ref. 32) (dashed line), and *ab initio* MD by Shimojo *et al.* (Ref. 33) (dotted line).

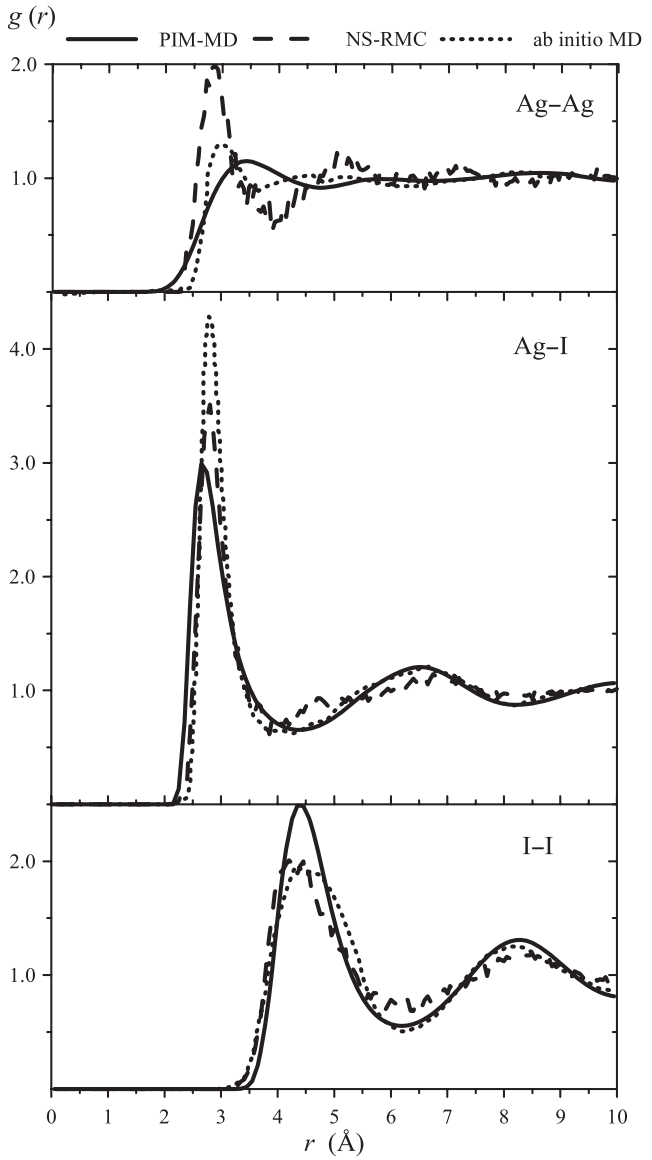

FIG. 6. The radial distribution functions $g_{AgAg}(r)$ (top), $g_{AgI}(r)$ (middle), and $g_{II}(r)$ (bottom) for molten AgI from PIM-MD of this work (solid line), NS-RMC by Kawakita *et al.* (Ref. 32) (dashed line), and *ab initio* MD by Shimojo *et al.* (Ref. 33) (dotted line).

of the $g_{AgAg}(r)$ from PIM-MD is at about 3.4 Å, between the first peak positions of $g_{AgI}(r)$ and $g_{II}(r)$, while the first peak of the $g_{AgAg}(r)$ from *ab initio* and NS-RMC is at about 3.0 Å, almost the same position of the $g_{AgI}(r)$ first peak.

The profile of the PIM-MD $g_{AgAg}(r)$ for molten AgI is very similar to that described above for molten AgCl, in such a way that the origin of the first and second maxima in the $S_{AgAg}(k)$ for AgI is the same as that for AgCl. However, while the PIM-MD $S_{AgAg}(k)$ exhibits a prepeak at about 1 Å^{-1} for molten AgI, this feature is not seen in molten AgCl. These results illustrate the fact that the intermediate-range spatial correlations between cations, which are pointed out in the reciprocal space by the $S_{AgAg}(k)$ prepeak for molten AgI, can not be identified in $g_{AgAg}(r)$.[43,44] Nevertheless, in the AgCl case, the values at around 1 Å^{-1} of the PIM-MD $S_{AgAg}(k)$ are higher than those from RIM-MD. That is, the intermediate-range polarization effects are also present in the PIM for AgCl but less clearly than in the PIM for AgI because $\alpha_{Cl} < \alpha_I$. Furthermore, since $b_{Cl} > b_I$, the weighted contribution of $S_{AgAg}(k)$ to $S(k)$ given in Eq. (7) is lower in AgCl than in AgI. Hence, in the AgCl $S(k)$, it is still more difficult to find any signature of the intermediate-range polarization effects on the cationic structure.

C. Structure of molten $Ag(Cl_{0.43}I_{0.57})$

The $S(k)$ for molten $Ag(Cl_{0.43}I_{0.57})$ at 743 K from PIM-MD is compared in Fig. 7 with those obtained from NS measurements by Takeda *et al.*[45,46] and by Kawakita *et al.*[30] While the earlier NS data by Takeda *et al.* were obtained with a monochromatic neutron beam and a two axis diffractometer, those by Kawakita *et al.* were obtained more recently with a pulse neutron and a time of flight spectrometer.

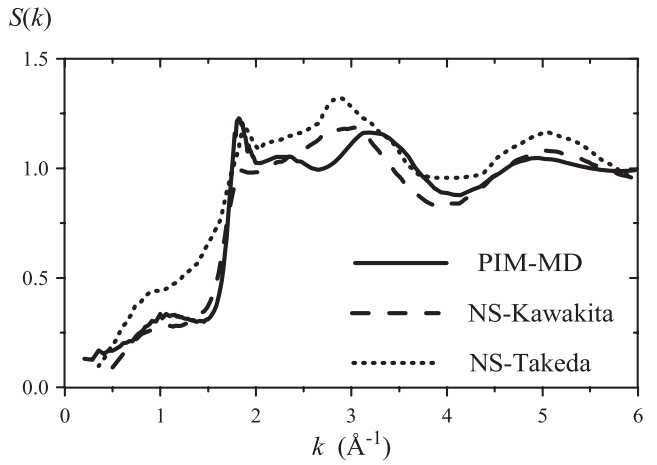

FIG. 7. The structure factor $S(k)$ for molten $Ag(Cl_{0.43}I_{0.57})$ from PIM-MD of this work (solid line) and NS measurements by Kawakita *et al.* (Ref. 30) (dashed line) and by Takeda *et al.* (Ref. 45) (dotted line).

The three $S(k)$ plotted in Fig. 7 exhibit the prepeak at about 1 $Å^{-1}$ characteristic of molten AgI and present a broad main peak with a spiky feature at about 1.8 $Å^{-1}$. The profile of the broad main peak in the $S(k)$ by Kawakita *et al.* is intermediate to that found in their $S(k)$ for molten AgCl and AgI. Following the spiky feature at about 1.8 $Å^{-1}$, it increases, more slowly than in AgI, up to the highest value at about 3.0 $Å^{-1}$. The profile of the broad main peak in the $S(k)$ from PIM-MD, which presents a middle hump at about 2.2 $Å^{-1}$ between a spiky peak and a maximum at about 3.2 $Å^{-1}$, is also intermediate to that obtained from PIM-MD for molten AgCl and AgI. It appears that the overestimated three-peak structure in PIM-MD for AgCl also dominates in the mixture. The prepeak at about 1 $Å^{-1}$ in the NS data for molten $Ag(Cl_{0.43}I_{0.57})$ is not observed, at least clearly enough, in the eutectic mixture between AgBr and AgI,[36] i.e., $Ag(Br_{0.7}I_{0.3})$. It could be due to the fact that the AgI concentration is lower in the latter mixture.

It is worth noting that the values at the lowest wave numbers of the PIM-MD $S(k)$ for the mixture are higher than those for the pure molten salts. It is because, while the long wavelength limit of the $S(k)$ for binary ionic systems such as AgCl and AgI is proportional to the compressibility, that for ternary ionic systems such as their mixture includes an extra term related to the dilatation factor and the mean square thermal fluctuations of the relative concentration of anions.[47]

In spite of the differences between the experimental and simulated $S(k)$, the main features of $S(k)$ are present in the simulations and therefore we assume that the simulated $g_{ab}(r)$ and $S_{ab}(k)$ presented in Figs. 8 and 9 are indicative of what may be expected. The simulated $g_{ab}(r)$ show that the ionic distribution in molten $Ag(Cl_{0.43}I_{0.57})$ is very similar to that in pure AgCl and AgI melts: an anion is surrounded by alternated shells of opposite charged ions, while the charge ordering around a cation is in some sense broken because the cations penetrate deeply into the first coordination shell of anions around a cation and the cationic distribution is less structured. Furthermore, since the chlorides are smaller than the iodides, in the first coordination shell of anions around a

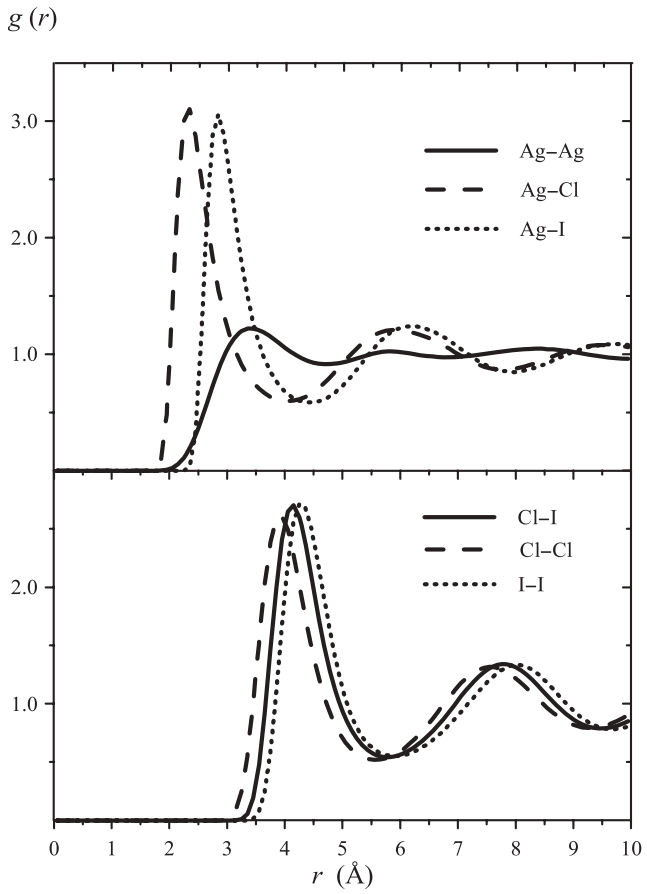

FIG. 8. The radial distribution functions for molten $Ag(Cl_{0.43}I_{0.57})$ from PIM-MD. Upper panel: $g_{AgAg}(r)$ (solid line), $g_{AgCl}(r)$ (dashed line), and $g_{AgI}(r)$ (dotted line). Lower panel: $g_{ClI}(r)$ (solid line), $g_{ClCl}(r)$ (dashed line), and $g_{II}(r)$ (dotted line).

silver ion the chlorides are nearer to the silver ion than the iodides and the averaged distance between two neighboring chlorides is smaller than that between two neighboring iodides. An accurate comparison between each $g_{ab}(r)$ for the simulated mixture and the corresponding $g_{ab}(r)$ for the pure molten salt shows that they are very similar, although small changes in the position and height of the first peak.

The Ashcroft–Langreth partial structure factors $S_{ab}(k)$ for molten $Ag(Cl_{0.43}I_{0.57})$ are shown in Fig. 9. The $S_{AgAg}(k)$ for the mixture is very close to that for molten AgI, i.e., it exhibits the prepeak and two relative maxima. At first glance, the $S_{AgCl}(k)$ and $S_{AgI}(k)$ for the mixture recall those for molten AgCl and AgI, but the main valley is less deep for the mixture. This difference comes from the Ashcroft–Langreth structure factors definition, which can be written as $S_{ab}(k) = \delta_{ab} + \rho(c_a c_b)^{1/2} h_{ab}(k)$, where $h_{ab}(k)$ is the spatial Fourier transform of $[g_{ab}(r) - 1]$. Hence, the $g_{ab}(r)$ contribution is weighted by $(c_a c_b)^{1/2}$, which is lower in the mixture. For instance, $(c_{Ag}c_{Cl})^{1/2} = 0.328$ in the mixture, whereas $(c_{Ag}c_{Cl})^{1/2} = 0.5$ in molten AgCl. Concerning the $S_{ClCl}(k)$ and $S_{II}(k)$ for the mixture, at first glance they also recall those for molten AgCl and AgI, but the main peak is lower for the mixture because of the weighting factor $(c_a c_b)^{1/2}$. Moreover, $S_{ClI}(k)$ also resembles $S_{ClCl}(k)$ and $S_{II}(k)$ but shifted vertically by -1. It is because the Kroncker's delta contribution in $S_{ClI}(k)$ is δ_{ClI}

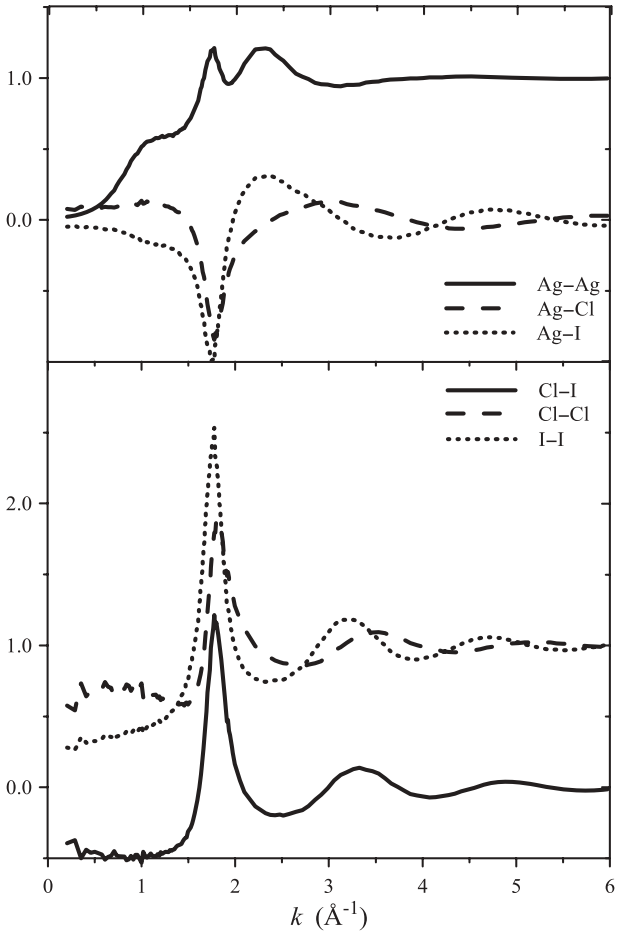

FIG. 9. The Ashcroft–Langreth partial structure factors for molten $Ag(Cl_{0.43}I_{0.57})$ from PIM-MD. Upper panel: $S_{AgAg}(k)$ (solid line), $S_{AgCl}(k)$ (dashed line), and $S_{AgI}(k)$ (dotted line). Lower panel: $S_{ClI}(k)$ (solid line), $S_{ClCl}(k)$ (dashed line), and $S_{II}(k)$ (dotted line).

$= 0$. However, the $S_{ClCl}(k)$ and $S_{II}(k)$ for the mixture at low k's are not close to 0 as in the pure melt. It is because, while the long wavelength limit of the $S_{ab}(k)$ for binary ionic systems are proportional to the compressibility, those for ternary ionic systems includes an extra term (see Ref. 47) in such a way that $S_{ClCl}(k \to 0) \approx x_{AgI} = 0.43$, $S_{II}(k \to 0) \approx x_{AgCl} = 0.57$, and $S_{ClI}(k \to 0) \approx -(x_{AgCl}\, x_{AgI})^{1/2} = -0.477$, as can be seen in Fig. 9.

V. CONCLUSIONS

We have studied the structure of molten AgCl and AgI as well as their eutectic mixture $Ag(Cl_{0.43}I_{0.57})$, by means of MD simulations of polarizable ion model potentials (PIM-MD). These model potentials result from adding the anion polarizability to simple rigid ion pair potentials of the form proposed by Vashishta and Rahman. The PIM-MD of molten AgI reproduce very well the experimental structure factor $S(k)$ with a prepeak at about 1 $Å^{-1}$ and a broad main peak between a small spiky feature at about 1.7 $Å^{-1}$ and the highest value at about 2.9 $Å^{-1}$. In the AgCl case, although the three-peak fine structure of the broad main peak in the $S(k)$ is overestimated, the agreement between the experimental and PIM-MD is fair good, at least better than for simple rigid ion model potentials. Concerning the eutectic mixture, the PIM-MD reproduce the prepeak at about 1 $Å^{-1}$ but the three-peak fine structure of the broad main peak is also overestimated.

The qualitative behavior of the simulated partial structure factors and the radial distribution functions for molten AgCl and AgI is that predicted by the reverse Monte Carlo modeling of the corresponding neutron scattering data. While an anion is surrounded by alternated shells of opposite charged ions, the cations structure is less ordered. *Ab initio* molecular dynamics of molten AgI also show these trends. From PIM-MD results it is concluded that the cationic coulomb ordering is in some sense broken because the repulsion between cations is screened by the electric field due to the induced dipoles in the anions.

ACKNOWLEDGMENTS

We thank Kawakita *et al*. the tabulated data of their experimental and RMC results in Refs. 30–32 used in this paper. This work was supported by DGI of Spain (Grant No. FIS2009-13641-C02-01) and the DURSI of the Generalitat of Catalonia (Grant No. 2009SGR-1003).

[1] J. B. Boyce and B. A. Huberman, Phys. Rep. **51**, 189 (1979).
[2] D. A. Keen, J. Phys.: Condens. Matter **14**, R819 (2002).
[3] S. Hull, Rep. Prog. Phys. **67**, 123 (2004).
[4] P. Vashishta and A. Rahman, Phys. Rev. Lett. **40**, 1337 (1978).
[5] P. Vashishta and A. Rahman, in *Fast Ion Transport in Solids*, edited by P. Vashishta, J. N. Mundy, and G. K. Shenoy (North-Holland, Amsterdam, 1979).
[6] M. Parrinello, A. Rahman, and P. Vashishta, Phys. Rev. Lett. **50**, 1073 (1983).
[7] J. L. Tallon, Phys. Rev. B **38**, 9069 (1988).
[8] C. Seok and D. W. Oxtoby, Phys. Rev. B **56**, 11485 (1997).
[9] D. A. Keen, S. Hull, A. C. Barnes, P. Berastegui, W. A. Crichton, P. A. Madden, M. G. Tucker, and M. Wilson, Phys. Rev. B **68**, 014117 (2003).
[10] M. A. Howe, R. L. McGreevy, and E. W. J. Mitchell, Z. Phys. B **62**, 15 (1985).
[11] D. I. Page and J. Mika, J. Phys. C **4**, 3034 (1971).
[12] S. Eisenberg, J. F. Jal, J. Dupuy, P. Chieux, and M. Knoll, Philos. Mag. A **46**, 195 (1982).
[13] A. J. Stafford and M. Silbert, Z. Phys. B **67**, 31 (1987).
[14] H. Takahashi, S. Takeda, S. Harada, and S. Tamaki, J. Phys. Soc. Jpn. **57**, 562 (1988)
[15] A. J. Stafford, M. Silbert, J. Trullàs, and A. Giró, J. Phys.: Condens. Matter **2**, 6631 (1990). In this article the curves should be interchanged between Figs. 2 and 3 in order to match the figure captions.
[16] J. E. Drewitt, P. S. Salmon, S. Takeda, and Y. Kawakita, J. Phys.: Condens. Matter **21**, 075104 (2009).
[17] Ç. Tasseven, J. Trullàs, O. Alcaraz, M. Silbert, and A. Giró, J. Chem. Phys. **106**, 7286 (1997).
[18] J. Y. Derrien and J. Dupuy, Phys. Chem. Liq. **5**, 71 (1976).
[19] D. A. Keen, W. Hayes, and R. L. McGreevy, J. Phys.: Condens. Matter **2**, 2773 (1990).
[20] M. Inui, S. Takeda, Y. Shirakawa, S. Tamaki, Y. Waseda, and Y. Yamaguchi, J. Phys. Soc. Jpn. **60**, 3025 (1991).
[21] M. Wilson, P. A. Madden, and B. J. Costa-Cabral, J. Phys. Chem. **100**, 1227 (1996).
[22] J. E. Mayer, J. Chem. Phys. **1**, 327 (1933).
[23] J. Trullàs, O. Alcaraz, and M. Silbert, J. Non-Cryst. Solids **312–314**, 438 (2002).
[24] J. Trullàs, O.Alcaraz, L. E. González, and M. Silbert, J. Phys. Chem. B **107**, 282 (2003).
[25] V. Bitrián and J. Trullàs, J. Phys. Chem. B **110**, 7490 (2006).
[26] V. Bitrián, J. Trullàs, and M. Silbert, J. Chem. Phys. **126**, 021105 (2007).
[27] V. Bitrián and J. Trullàs, J. Phys. Chem. B **112**, 1718 (2008).
[28] V. Bitrián and J. Trullàs, J. Phys.: Conf. Ser. **98**, 0242006 (2008).

[29]V. Bitrián, O. Alcaraz, and J. Trullàs, J. Chem. Phys. **130**, 234504 (2009).
[30]Y. Kawakita, T. Enosaki, S. Takeda, and K. Maruyama, J. Non-Cryst. Solids **353**, 3035 (2007).
[31]S. Tahara, H. Fujii, Y. Kawakita, S. Kohara, Y. Yokota, and S. Takeda, J. Non-Cryst. Solids **353**, 1994 (2007).
[32]Y. Kawakita, S. Tahara, H. Fujii, S. Kohara, and S. Takeda, J. Phys.: Condens. Matter **19**, 335201 (2007).
[33]F. Shimojo, T. Inoue, M. Aniya, T. Sugahara, and Y. Miyata, J. Phys. Soc. Jpn. **75**, 114602 (2006)
[34]S. Takeda, Y. Nagata, and Y. Kawakita, J. Non-Cryst. Solids **353**, 3169 (2007) and references therein.
[35]F. Shimojo and M. Kobayashi, J. Phys. Soc. Jpn. **60**, 3725 (1991).
[36]V. Bitrián, J. Trullàs, M. Silbert, T. Enosaki, Y. Kawakita, and S. Takeda, J. Chem. Phys. **125**, 184510 (2006).
[37]G. J. Janz, F. W. Dampier, G. R. Lakshminarayanan, P. K. Lorenz, and R. P. T. Tomkins, *Molten Salts: Volume 1 Electrical Conductance, Density, and Viscosity Data* (National Standard Reference Data Series–National Bureau of Standards 15, U.S. Government Printing Office, Washington, D.C., 1968.)
[38]M. P. Tosi, D. L. Price, and M.-L. Saboungi, Annu. Rev. Phys. Chem. **44**, 173 (1993).
[39]V. F. Sears, Neutron News **3**, 26 (1992); see also online at http://www.ncnr.nist.gov/resources/n-lengths/.
[40]H. E. Fisher, A. C. Barnes, and P. S. Salmon, Rep. Prog. Phys. **69**, 233 (2006).
[41]M. Rovere and M. P. Tosi, Rep. Prog. Phys. **49**, 1001 (1986).
[42]Y. Shirakawa, S. Tamaki, T. Usuky, K. Sugiyama, and Y. Waseda, J. Phys. Soc. Jpn. **63**, 1814 (1994).
[43]S. R. Elliot, Phys. Rev. Lett. **67**, 711 (1991).
[44]P. S. Salmon, Proc. Roy. Soc. Lond. A **445**, 351 (1994).
[45]S. Takeda, Y. Kawakita, and M. Inui, High Temp. Mater. Processes **18**, 65 (1999).
[46]S. Takeda, Y. Kawakita, M. Inui, and K. Muruyama, J. Non-Cryst. Solids **250-252**, 410 (1999).
[47]V. Bitrián, J. Trullàs, and M. Silbert, Physica B **403**, 4249 (2008).